Condensation of Silicon Carbide in Supernova Ejecta

The Astrophysical Journal, 843:57 (8pp), 2017 July 1 https://doi.org/10.3847/1538-4357/aa7753

Condensation of Silicon Carbide in Supernova Ejecta

Ethan Deneault
University of Tampa, 401 W. Kennedy Blvd., Tampa, FL 33606, USA; edeneault@ut.edu
Received 2017 April 25; revised 2017 May 24; accepted 2017 June 1; published 2017 July 3

Abstract

We present a kinetic model of the formation of silicon carbide (SiC) in the expanding and cooling outflows of Type II supernova ejecta. We assume an ejecta cloud composed of a mixture of Si, C, and O in the gas phase, with the initial temperature, density, and composition as tunable parameters. The condensation of diatomic SiC into $(SiC)_2$ molecules provides the abundance of nucleation sites for the eventual condensation of larger SiC solids and dust grains. We find that the abundance of these nucleation sites, formed after the first 1700 days after the explosion, is strongly governed by the C/Si ratio, the density of the gas, and the rate of cooling in the ejecta.

Key words: astrochemistry – ISM: supernova remnants – molecular processes

1. Introduction

Understanding the origin of dust in the universe is an important question in astrophysics. Laboratory studies of dust grains extracted from primordial meteorites have been used to probe the chemical composition and conditions in the outflows of AGB stars and supernovae. Approximately 1% of the silicon carbide (SiC) grains studied have peculiar isotopic signatures that identify their origin in type II supernovae (Nittler et al. 1996; Clayton & Nittler 2004). That supernovae produce large amounts of dust has been controversial, since detailed investigations of the IR spectra of supernova ejecta had shown evidence of only a small abundance ($\sim 10^{-2}\,M_{\odot}$) of warm dust (Sugerman et al. 2006; Ercolano et al. 2007). More recently, however, observations condicted with the *Herschel* telescope have discovered a much larger reservoir (0.4–0.7 $M_{\odot}$) of cold dust in SN 1987A (Matsuura et al. 2011) as well as in Cas A (De Looze et al. 2017). Evidence of the rapid formation of dust grains (Gall et al. 2014) supports the idea that supernovae can produce dust quickly and efficiently (Clayton et al. 2001; Todini & Ferrara 2001; Nozawa et al. 2003).

The discovery of SiC grains of supernova origin in particular requires further explanation. Deneault et al. (2003) argued that SiC must form within the ejecta in regions where the Si/C ratio is greater than 10, otherwise free C will be depleted into C grains. However, although the signature 11.3 μm spectral feature of SiC is seen in the circumstellar region of AGB stars or C stars (Kozasa et al. 1996), this feature has not been detected in supernovae to date. Previous investigations of the formation of SiC were inconclusive, showing no SiC condensation at all (Nozawa et al. 2003; Cherchneff & Dwek 2010). How then do SiC-X grains form? In this study, we investigate the formation of SiC and the conditions required for its condensation in the ejecta.

2. The Ejecta Model

Previous models of condensation in supernovae have assumed that the ejecta is either fully mixed (Nozawa et al. 2003) or in one-dimensional spherically symmetric shells with an unmixed composition (Deneault et al. 2006; Cherchneff & Dwek 2010). Observations of supernova ejecta (Fesen 2001) and multi-dimensional models of supernova explosions (Kifonidis et al. 2003; Hammer et al. 2010; Wongwathanarat et al. 2015) strongly imply that Rayleigh–Taylor instabilities can form between the boundary layers of these shells, and clumps of material from the denser inner regions of the ejecta can be projected outward (in mass coordinate) to lighter-mass regions of the ejecta. We can therefore envision the ejecta as less of an "onion," with layers of material overlaid on top of each other, and more as a partially mixed collection of gas clouds of varying composition.

This macroscopic mixing of the ejecta is in contrast to microscopic mixing due to diffusion, which is much slower (Deneault et al. 2003). However, the observed isotopic composition of meteoritic supernova condensates requires that some microscopic mixing occur. The inferred presence of ^{26}Al in an SiC-X grain, as an example, requires material found in the outer He-rich layer, but Si requires material from much deeper regions (Clayton & Nittler 2004). By necessity, mixing in the ejecta must be limited; a fully microscopically mixed ejecta will produce no C grains at all. Destructive reactions with He^{+} ions disrupt the formation of molecules early on (Cherchneff & Dwek 2010). However, the timescale for the complete mixing of the entire ejecta through diffusion is far longer than the timescale for the grain formation (Deneault et al. 2003). Microscopic mixing therefore occurs most likely around the edges of the instabilities between different compositional regions (Arnett et al. 1989).

2.1. Density and Thermal Environments

In this study we model a single cloud of material in the ejecta with a given initial composition. Although it is not our goal to model a specific supernova, we do constrain our interest to compositions that are "reasonable" for massive stars, using the models of Rauscher et al. (2002) as a guide. We define the number density of the gas in our cloud to be equal to the number of initial gas atoms in the system per unit volume. The expansion of the cloud proceeds in a homologous fashion, so that the number density of gas particles in the shell decreases in time as

$$n(t) = n_0 \left(\frac{t}{t_0}\right)^{-3}. \quad (1)$$

We take the standard number density of the gas to be given by $n_0 = 2.544 \times 10^9\ \mathrm{cm}^{-3}$ at the fiducial time $t_0 = 100$ days, but an individual gas cloud may have a higher or a lower density.

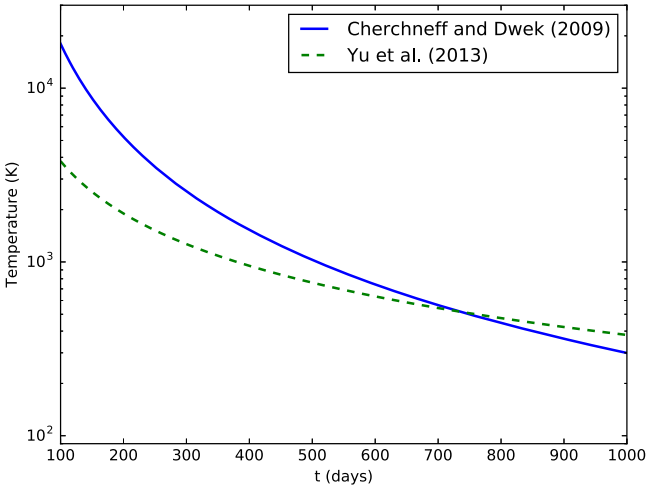

Figure 1. Comparison of the temperature models used by the chemical network. The YCM model varies over an order of magnitude during the first 1000 days post-explosion, and remains much warmer at long times compared to the CD model.

We choose to model the thermal environment of the ejecta using two different models: the 20 $M_\odot$ CC supernova model from Cherchneff & Dwek (2009; the CD model) and the temperature model used by Deneault et al. (2006) and by Yu et al. (2013; the YCM model). For both models, the evolution of the ejecta temperature in time is given by the relation

$$T(t) = T_0 \left(\frac{t}{t_0}\right)^{3(1-\gamma)}, \quad (2)$$

where γ is a parameter specific to the temperature model used.

The CD model assumes that the ejecta follows a quasi-adiabatic expansion, and those authors originally chose $\gamma = 1.593$ to match the temperature profile from Nozawa et al. (2003). The CD model chooses $T_0 = 18{,}000$ K to be the temperature at 100 days post-explosion (see Cherchneff & Dwek 2009, Figure 1).

In contrast, model YCM (Yu et al. 2013) assumes the significant CO cooling in the ejecta shown by Liu & Dalgarno (1996) so that the temperature at 100 days is 3800 K, a factor of nearly one fifth of the CD model at that time. This model takes the factor $\gamma = 4/3$ in Equation (2), which leads to a much slower decrease in temperature over time.

Figure 1 plots both temperature models over the first 1000 days post-explosion. Although the CD model begins at a much higher temperature, the temperature drops very sharply, reaching the initial temperature of the YCM model after approximately 250 days post-explosion and dropping below the YCM model at about 750 days.

3. Reaction Network

We restrict our network to the three atomic species that are the most important to the formation of SiC molecules: C, O, and Si, as well as diatomic and multiatomic molecules made up of these species. In total, there are 32 atomic, molecular, and ionic species included in the network, tabulated in Table 1. Since our present goal is not to model the condensation process of solids in the ejecta but to investigate the conditions for the formation of SiC, we have chosen the abundance of the $(SiC)_2$ molecule to represent the abundance of nucleation sites for the formation of SiC grains. Our model assumes that the $(SiC)_2$ as well as the $(SiO)_2$ molecules are stable except at high temperatures. These molecules therefore allow us to trace the number of "seed nuclei" for the eventual growth of dust grains in the ejecta.

Table 1
Atomic and Molecular Species Included in the Network

Type	Species
atoms	C, O, Si
molecules	CO, O_2, SiO, SiC, C_2, C_3, C_4, C_5, C_6, C_7, C_8, $(SiC)_2$, $(SiO)_2$
ions	C^+, O^+, Si^+, CO^+, SiO^+, SiC^+, C_2^+

The abundance of a given species N_i in the gas phase is governed by a rate equation of the form

$$\frac{dN_i}{dt} = \sum_{j\ell} k_{j\ell} N_j N_\ell - \sum_{\ell} k_{i\ell} N_i N_\ell + \sum_{j} k_j N_j - \sum_{\ell} k_\ell N_i, \quad (3)$$

where the first two terms represent bimolecular reactions that create or destroy the species and the second two terms represent unimolecular reactions. Although termolecular reactions are possible in the gas phase, we have not included them in the network in order to simplify our calculation.

The network contains approximately 100 individual reactions between one or two species. The reaction rate $k = k(T)$ is a temperature-dependent coefficient described by the modified Arrhenius equation:

$$k(T) = \alpha \left(\frac{T}{300}\right)^{\beta} e^{-\gamma/T}, \quad (4)$$

where the coefficient α is given in units of $cm^3\,s^{-1}$ for bimolecular reactions and in units of s^{-1} for unimolecular reactions, and the coefficient $\gamma = E_a/k_B$ is the defined activation energy of the reaction divided by Boltzmann's constant. The values of α, β, and γ are dependent on the probabilities of interaction between the reactants and are therefore reaction-specific. The reaction coefficients used in this study come from the comprehensive list found in Cherchneff & Dwek (2009, 2010) and include updated values from the UMIST12 database (McElroy et al. 2013), the KIDA database (Wakelam et al. 2012), and other sources individually referenced in Tables 2–8.

The coupled equations in Equation (3) governing the formation of molecules in the ejecta are modeled using the *CarBoNpy* kinetic reaction network, developed by the author. This code is designed for the input of various ejecta model parameters, chemical species, and reactions and has been successfully tested against previously published works.

3.1. Thermal and Nonthermal Disruption

Small molecules in the ejecta are particularly susceptible to disruption from nonthermal Compton electrons created by the scattering of gamma rays from the decay of ^{56}Co (Clayton et al. 1999). We have adopted the Compton electron destruction rates for diatomic species from Cherchneff & Dwek (2009), taking the Compton electron destruction rates for SiC to be comparable to those for SiO.

Table 2
Radiative Association Reactions

Name	Reactants	Products	α	β	γ	Source
R1	$C + C$	$C_2 + \gamma$	4.36×10^{-18}	0.35	161.3	UMIST12
R2	$C + C_2$	$C_3 + \gamma$	3×10^{-16}	−1	0	UMIST12
R3	$C + C_3$	$C_4 + \gamma$	4×10^{-14}	−1	0	UMIST12
R4	$C + C_4$	$C_5 + \gamma$	1×10^{-13}	−1	0	Clayton et al. (1999)
R5	$C + C_5$	$C_6 + \gamma$	1×10^{-10}	−1	0	Clayton et al. (1999)
R6	$C + C_6$	$C_7 + \gamma$	1×10^{-13}	−1	0	Clayton et al. (1999)
R7	$C + C_7$	$C_8 + \gamma$	1×10^{-10}	−1	0	Clayton et al. (1999)
R8	$C + O$	$CO + \gamma$	1.482×10^{-17}	0.54	329	KIDA
R9	$O + O$	$O_2 + \gamma$	1×10^{-19}	0	0	Cherchneff & Dwek (2009)
R10	$Si + C$	$SiC + \gamma$	2.038×10^{-17}	-1.263×10^{-2}	136.73	Andreazza et al. (2009)
R11	$Si + O$	$SiO + \gamma$	5.520×10^{-18}	0.31	0	UMIST12

Table 3
Neutral–Neutral Reactions

Name	Reactants	Products	α	β	γ	Source
N1	$C + CO$	$C_2 + O$	1.0×10^{-10}	0	52800	KIDA
N2	$C + O_2$	$CO + O$	5.56×10^{-11}	0.41	−26.90	UMIST12
N3	$C + C_4$	$C_2 + C_3$	2.4×10^{-10}	0	0	KIDA
N4	$C + C_5$	$C_3 + C_3$	1.5×10^{-10}	0	0	KIDA
N5	$C + C_6$	$C_4 + C_3$	2.0×10^{-10}	0	0	KIDA
N6	$C + C_6$	$C_5 + C_2$	4.0×10^{-11}	0	0	KIDA
N7	$C + C_7$	$C_3 + C_5$	2.0×10^{-10}	0	0	KIDA
N8	$C + C_8$	$C_7 + C_2$	1.0×10^{-11}	0	0	KIDA
N9	$C + C_8$	$C_6 + C_3$	1.6×10^{-10}	0	0	KIDA
N10	$C + C_8$	$C_5 + C_4$	7.0×10^{-11}	0	0	KIDA
N11	$C + SiO$	$Si + CO$	1.0×10^{-16}	0	0	Cherchneff & Dwek (2009)
N12	$C + SiO$	$SiC + O$	1.0×10^{-10}	0	52800	same as N1[a]
N13	$O + C_2$	$CO + C$	3.0×10^{-10}	−0.12	0	UMIST12
N14	$O + C_3$	$CO + C_2$	5.0×10^{-12}	0	900	UMIST12
N15	$O + C_4$	$CO + C_3$	1.0×10^{-10}	0.17	0	KIDA
N16	$O + C_5$	$CO + C_4$	5.0×10^{-12}	0	900	UMIST12
N17	$O + C_6$	$CO + C_5$	1.0×10^{-10}	0.17	0	KIDA
N18	$O + C_7$	$CO + C_6$	5.0×10^{-12}	0	900	UMIST12
N19	$O + C_8$	$CO + C_7$	1.0×10^{-10}	0.17	0	KIDA
N20	$O + SiC$	$Si + CO$	5.0×10^{-11}	0	0	KIDA
N21	$O + SiC$	$SiO + C$	5.0×10^{-11}	0	0	KIDA
N22	$O + CO$	$O_2 + C$	1.0×10^{-16}	0	0	Cherchneff & Dwek (2009)
N23	$O + SiO$	$O_2 + Si$	1.0×10^{-16}	0	0	Cherchneff & Dwek (2009)
N24	$Si + C_2$	$SiC + C$	5.99×10^{-10}	0	1420	Cherchneff & Dwek (2010)
N25	$Si + CO$	$SiO + C$	1.3×10^{-9}	0	34516	UMIST12
N26	$Si + CO$	$SiC + O$	1.0×10^{-10}	0	52800	same as N1[a]
N27	$Si + O_2$	$SiO + O$	1.72×10^{-10}	−0.53	17	Cherchneff & Dwek (2009)

Note.
[a] We follow Cherchneff & Dwek (2009) in assigning these reactions rates as equal.

Table 4
Compton Electron Reactions

Name	Reactants	Products	α	β	γ	Source
C1	SiC	$Si + C$	6.58×10^{-6}	0	3464.1	See note
C2	SiC	$Si^+ + C + e^-$	3.33×10^{-6}	0	3464.1	”
C3	SiC	$Si + C^+ + e^-$	1.07×10^{-7}	0	3464.1	”
C4	SiC	$SiC^+ + e^-$	2.42×10^{-5}	0	3464.1	”

Note. These rates are estimated from Cherchneff & Dwek (2009). All other rates for interactions with Compton electrons can be found in Table 5 of that paper.

Table 5
Electron Recombination Reactions

Name	Reactants	Products	α	β	γ	Source
ER1	$C^+ + e^-$	$C + \gamma$	2.36×10^{-12}	−0.29	−17.6	UMIST12
ER2	$O^+ + e^-$	$O + \gamma$	3.24×10^{-12}	−0.66	0	”
ER3	$Si^+ + e^-$	$Si + \gamma$	4.26×10^{-12}	−0.62	0	”
ER4	$C_2^+ + e^-$	$C + C$	3.0×10^{-7}	−0.50	0	”
ER5	$CO^+ + e^-$	$C + O$	2.0×10^{-7}	−0.48	0	”
ER6	$SiO^+ + e^-$	$Si + O$	2.0×10^{-7}	−0.5	0	”
ER7	$SiC^+ + e^-$	$Si + C$	2.0×10^{-7}	−0.5	0	”

Table 6
Ion-Molecule Reactions and Charge Exchange Reactions

Name	Reactants	Products	α	β	γ	Source
I1	$C + O^+$	CO^+	5.0×10^{-10}	−3.7	800	UMIST12
I2	$C + C_2^+$	$C_2 + C^+$	1.10×10^{-10}	0	0	”
I3	$C^+ + C$	C_2^+	4.01×10^{-18}	0.17	101.5	”
I4	$C^+ + O_2$	$CO^+ + O$	3.42×10^{-10}	0	0	”
I5	$C^+ + O_2$	$CO + O^+$	4.54×10^{-10}	0	0	”
I6	$C^+ + SiO$	$Si^+ + CO$	5.40×10^{-10}	−0.5	0	”
I7	$C^+ + SiC$	$Si^+ + C_2$	2.50×10^{-9}	−0.5	0	”
I8	$C_2 + SiO^+$	$SiC^+ + CO$	7.60×10^{-10}	0	0	”
I9	$C_2^+ + O_2$	$CO^+ + CO$	8.0×10^{-10}	0	0	”
I10	$O + C^+$	CO^+	3.14×10^{-18}	−0.15	68.0	”
I11	$O + C_2^+$	$CO^+ + C$	3.10×10^{-10}	0	0	”
I12	$O + SiO^+$	$O_2 + Si^+$	2.0×10^{-10}	0	0	”
I13	$O + SiC^+$	$SiO^+ + C$	6.0×10^{-10}	0	0	”
I14	$O^+ + C_2$	$CO^+ + C$	4.80×10^{-10}	0	0	”
I15	$C + CO^+$	$C^+ + CO$	1.10×10^{-10}	0	0	”
I16	$C + C_2^+$	$C^+ + C_2$	1.10×10^{-10}	0	0	”
I17	$C_2 + O^+$	$C_2^+ + O$	4.80×10^{-10}	0	0	”
I18	$O + CO^+$	$O^+ + CO$	1.40×10^{-10}	0	0	”
I19	$CO + O^+$	$CO^+ + O$	4.90×10^{-12}	0	0	”
I20	$Si + C^+$	$Si^+ + C$	2.10×10^{-9}	0	0	”

Table 7
Thermal Photodissociation Reactions

Name	Reactants	Products	α	β	γ	Source
T1	$CO + \gamma_{th}$	$C + O$	2.61×10^8	2.04	1.29×10^5	See text
T2	$C_2 + \gamma_{th}$	$C + C$	6.28×10^7	1.85	7.28×10^4	”
T3	$O_2 + \gamma_{th}$	$O + O$	2.22×10^6	1.50	5.97×10^4	”
T4	$SiO + \gamma_{th}$	$Si + O$	1.78×10^8	1.81	9.73×10^4	”
T5	$SiC + \gamma_{th}$	$Si + C$	4.86×10^8	1.48	5.44×10^4	”

Table 8
Dust Precursor Reactions

Name	Reactants	Products	α	β	γ	Source
DP1	$SiC + SiC$	$(SiC)_2$	4.60×10^{-17}	0	-2.82×10^3	Cherchneff & Dwek (2010)
DP2	$(SiC)_2 + M$	$SiC + SiC$	4.40×10^{-10}	0	9.86×10^3	”
DP3	$SiO + SiO$	$(SiO)_2$	4.60×10^{-17}	0	-2.82×10^3	”
DP4	$(SiO)_2 + M$	$SiO + SiO$	4.40×10^{-10}	0	9.86×10^3	”

Yu et al. (2013) stressed the importance of the thermal disruption of CO molecules at early times in the ejecta. When the ejecta temperature is very high, interaction with thermal photons is the primary destructive channel for CO molecules, leading to a significant early-time depletion of CO in the ejecta. In general, for any diatomic molecule, the time (in seconds)

Table 9
Abundance of $(SiC)_2$ in Atoms^{-1} at 1760 Days Post-explosion as a Function of the Initial Composition of the Gas

Zone	Initial Composition			Abundance (atoms^{-1})	
	C	O	Si	CD	YCM
A	0.01	1	0.1	2.034×10^{-14}	1.079×10^{-18}
B	0.01	1	0.01	1.060×10^{-16}	6.471×10^{-21}
C	0.01	1	0.005	2.207×10^{-17}	1.385×10^{-21}
D	0.1	1	0.1	3.949×10^{-12}	2.204×10^{-16}
E	0.1	1	0.01	3.166×10^{-14}	1.119×10^{-18}
F	0.1	1	0.001	1.932×10^{-18}	2.280×10^{-24}
G	1	1	0.1	4.649×10^{-10}	5.267×10^{-14}
H	1	1	0.01	4.668×10^{-12}	1.879×10^{-16}
I	1	0.1	1	2.106×10^{-6}	2.594×10^{-10}
J	1	0.02	0.1	5.863×10^{-7}	1.333×10^{-10}

Note. The initial composition is given in terms of the relative abundance of atomic species.

that the molecule will exist before disruption from a thermal photon is given by the detailed balance equation

$$\tau_\gamma = \left(\frac{h^2}{2\pi\mu k_B T}\right)^{3/2} \frac{1}{k_{rad}} e^{E_B/k_B T}, \quad (5)$$

where E_B is the binding energy of the molecule, μ is the reduced mass of the reaction, and k_{rad} is the radiative association rate for the molecule given by Equation (4). Disruption by a thermal photon is a unimolecular reaction, so the rate of reaction can be given by $k(T) = 1/\tau_\gamma$. Solving this equation and expanding it into Arrhenius form, we find for any diatomic molecule that the Arrhenius coefficients for thermal disruption are given by:

$$\alpha = \alpha'\left(\frac{600\,\pi\mu k_B}{h^2}\right)^{3/2} \quad (6)$$

$$\beta = \beta' + \frac{3}{2} \quad (7)$$

$$\gamma = \frac{E_B + k_B\gamma'}{k_B}, \quad (8)$$

using the tabulated coefficients for the specific radiative association reaction in Table 2 for α', β', and γ'. The calculated Arrhenius coefficients for thermal destruction can be found in Table 7.

Each of the calculated rates has extremely high leading coefficients (10^6–10^8) but the exponential factor decays very quickly with decreasing temperature. The net effect of thermal destruction channels is extreme at early times (see Section 4.4), but the greatest effect of thermal disruption all but vanishes once the gas temperature reaches around a few thousand K.

4. Results

4.1. Composition

We calculated the abundances of molecules in the gas across a range of initial compositions, characterized by the initial proportions of C, O, and Si in the initial gas phase with a total number density of $n = 10^{10}$ cm^{-3}. These conditions were chosen to be similar to the shell abundances in the 25 $M_\odot$ model of Woosley et al. (2002) and reasonable assumptions of some admixing between clumps of ejecta material. The abundance (in atoms^{-1}) of $(SiC)_2$ after 1700 days post-explosion is given in Table 9 for each initial composition zone and both temperature models.

The radiative formation of SiC is in direct competition with the formation of SiO, which we see as reactions R10 and R11 in Table 3 and is plotted in Figure 2 using the CD temperature model. For all time plotted, the rate of formation of SiC is higher than that of SiO, which indicates that if we consider only radiative association, then there should be a significantly larger amount of SiC condensed unless the O abundance is at least an order of magnitude higher than that of C.

The highest abundances in Table 9 are found in the C-rich ejecta zones I and J, which are analogous to the oxygen-poor He/C region in the ejecta. In this region, the lower abundance of O ameliorates its destructive effect on SiC (reactions N20 and N21 in Table 3), and the radiative formation of SiC dominates over SiO. A clump of Si-rich ejecta material with a C/O ratio that is much larger than unity will certainly condense SiC. The He/C region in the ejecta is extremely He rich, with the abundance of He a few orders of magnitude larger than that of C, O, and Si (Woosley et al. 2002). Interactions with He^+ ions do quickly destroy diatomic molecules (Cherchneff & Dwek 2009), likely offsetting any advantage that the O-poor environment provides to SiC formation.

In zones where the C/O ratio is at or much lower than unity, the total abundance of SiC decreases significantly due to the presence of highly reactive oxygen. In these zones, we find that the C/Si ratio is extremely important. When the C/Si ratio is close to unity, there is a much higher abundance of the $(SiC)_2$ molecule. This trend is apparent regardless of the C/O ratio of the gas and seems to confirms the prediction from Deneault et al. (2003) as to where the most likely region for SiC condensation occurs.

4.2. Ejecta Temperature

In this study, we have chosen to look at two different temperature models: the high-initial-temperature (18,000 K at 100 days) CD model and the YCM model, whose temperature at 100 days is a much lower 3800 K due to CO cooling. Unexpectedly, across all temperatures and zones we find remarkably similar abundances across all temperatures for most species in the network. The abundances in zone A are plotted in Figure 3—the solid line corresponds to the CD model and the dashed line corresponds to the YCM model. About a third of the reactions in the model are completely temperature-independent rates: $\beta = \gamma = 0$. These reactions occur in the same way regardless of the model that we used. The other reaction rates increase or freeze out at very high or very low temperatures. At early times, the high temperature of the CD model makes available reaction pathways that have a high activation energy, such as reactions N1 and N12 from Table 3, or reactions where $\beta > 0$. This leads to a sharp "bump" in the abundances at early times, or a slow rise to a near steady state. Reactions with $\beta < 0$ increase sharply as the temperature decreases below 300 K.

Of special note is the dramatic increase in the abundance of $(SiC)_2$ and $(SiO)_2$ in the CD model but not in the YCM model. At a temperature of $T = 789$ K, the rate of reactions DP1 and DP3 from Table 8 is exactly equal to the reactions DP2 and DP4, and below that critical temperature, the rate of condensation increases

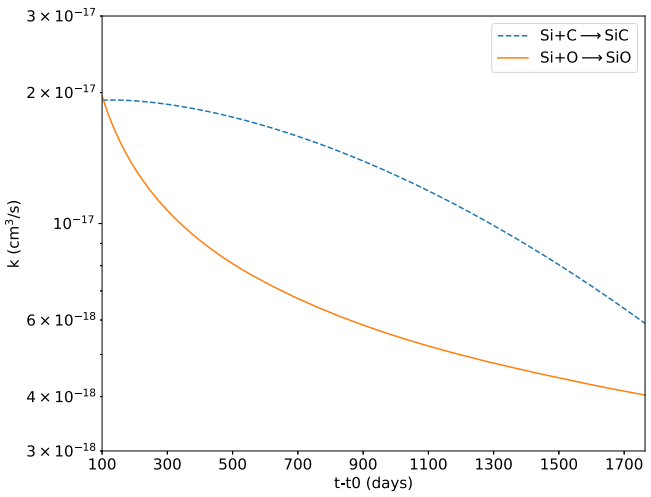

Figure 2. Radiative association rates for reactions R10 and R11 (Table 3) as a function of temperature using the CD temperature model.

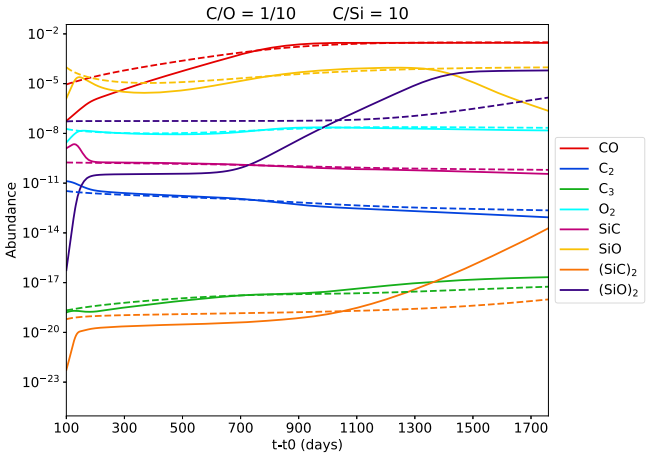

Figure 3. Comparison of abundances of selected species between days 100–1760 for the CD (solid line) and YCM (dashed line) temperature models. With the exception of the abundances of $(SiC)_2$ and $(SiO)_2$, there is very little difference in the overall abundances over time.

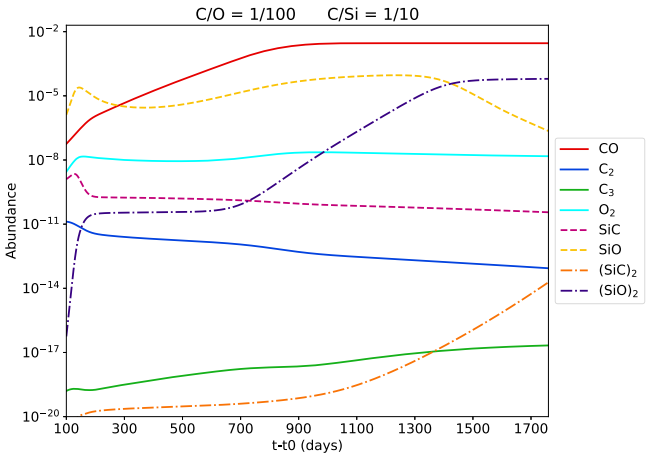

Figure 4. Abundances of selected molecular species over the first 1760 days post-explosion in the CD temperature model ejecta with $n_0 = 2.54 \times 10^9$ cm^{-3}.

quickly. The CD model drops below this critical temperature near 600 days, and we can see in Figure 3 that at around that time the abundance of $(SiO)_2$ begins its sharp rise. The increase for $(SiC)_2$

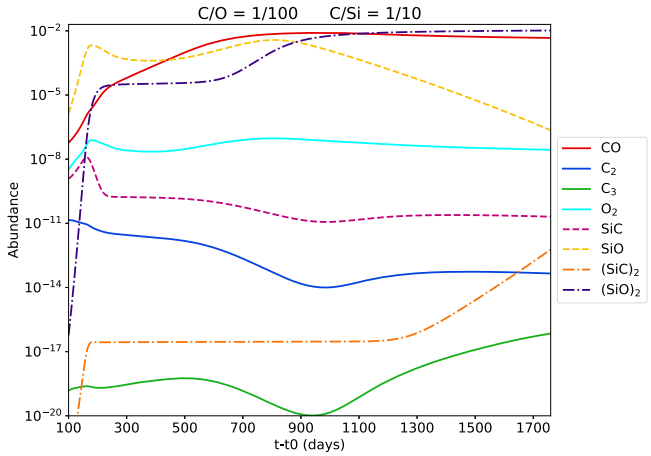

Figure 5. Abundances of selected molecular species over the first 1760 days post-explosion in the CD temperature model ejecta with an initial density of $n_0 = 2.54 \times 10^{11}$ cm^{-3}.

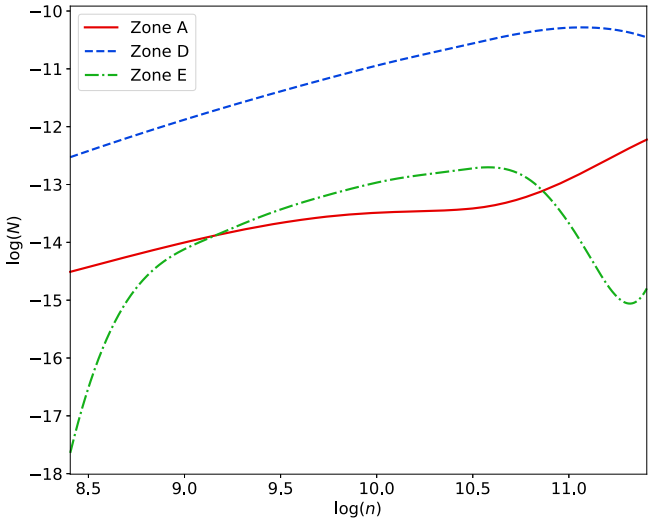

Figure 6. Log abundance N of $(SiC)_2$ at 1760 days as a function of the initial density n_0 in the gas. Zone A has a C/O ratio of 1/100 and a C/Si ratio of 1/10, Zone D has a C/O ratio of 1/10 and a C/Si ratio of 1, and Zone E has a C/O ratio of 1/10 and a C/Si ratio of 10. The abundances are highly dependent on both the composition and the density of the ejecta.

is delayed for a few hundred days due to the much lower abundance of SiC. The YCM model, although it initially has a cooler temperature, remains warmer than the CD model after 700 days, and the dramatic increases are not seen until nearer to 1600 days. Given that these nucleation sites preferably condense at lower temperatures, the quickly cooling CD model is preferable for producing dust precursors quickly compared to the slower-cooling YCM model.

4.3. Density

A typical supernova ejecta (such as Cas A) is highly nonuniform with denser knots surrounded by a more diffuse gas. The gas clouds modeled in this work could perhaps have densities that vary by an order of magnitude (or more) from the standard value that we chose in Section 2.1. Figures 4 and 5 plot the abundances of selected molecules as a function of time for zone A with a density of 2.54×10^9 and 2.54×10^{11} cm^{-3}.

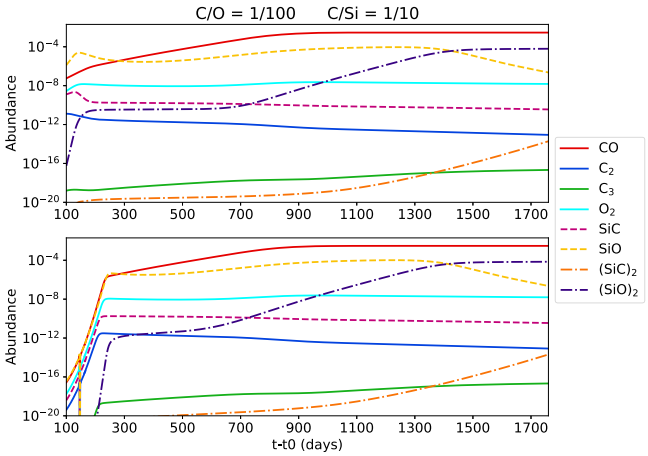

Figure 7. Abundances of selected molecular species over the first 1760 days post-explosion without thermal disruption (top) and with thermal destruction (bottom) in zone A. The thermal disruption of small molecules significantly retards the growth of molecules in the ejecta for approximately 200 days, but has little effect on the abundances at long times.

At the higher density, O quickly traps the free C in the system so that the steady-state abundance of CO is reached earlier than at the lower density. The increase in gas density has a notable effect on the Si-bearing molecules—higher-density gas immediately leads to a higher abundance for both SiO and SiC, with a significant fraction of Si atoms trapped in $(SiO)_2$ at the higher density.

Figure 6 shows the abundance N of $(SiC)_2$ at 1760 days plotted as a function of the number density n_0 for zones A, D, and E. For both zones A and D, the general trend shows that the abundance increases with density. One surprising result is the plateau in zone A that occurs at a density near 10^{10} cm^{-3}. It is not immediately clear why the abundances are relatively insensitive to density in this range. The formation of $(SiC)_2$ is directly dependent on the abundance of diatomic SiC that is available to condense. The formation of diatomic SiC competes directly with the much faster destructive reactions N20 and N21 from Table 3. Due to the lower C/Si ratio in zone A, at densities between 10^{10} and 1.5×10^{10} cm^{-3} the higher rate of production of SiC is balanced by a higher rate of destruction. At higher densities, near 10^{11} cm^{-3}, the formation of diatomic SiC outpaces its destruction. The abundances in zone E follow a completely different trend, producing maximal $(SiC)_2$ at midrange densities but far less at higher and at lower densities. These results show clearly that a C-rich gas produces substantially more SiC at densities near 10^{10} cm^{-3} than one that is Si rich, but a region where C/Si = 1 produces the most SiC by two orders of magnitude across all densities.

4.4. Thermal Disruption

The thermal disruption of small molecules dominates the abundance of molecules at an early time, which we can see in Figure 7. With the high-initial-temperature CD model, thermal disruption greatly retards the formation of molecules in the ejecta for the first ∼200 days post-explosion, until the temperature drops to about 4000 K (see Figure 1). At this temperature, the lifetime of a molecule against thermal disruption is very long and chemistry dominates the molecular reactions.

It is interesting to note that the early thermal disruption has almost no effect on the abundances of molecules at long times (>800 days). The net effect of thermal photons, therefore, is to delay the onset of condensation until the temperature of the ejecta is low enough for diatomic molecules to condense and survive. The most important effects are in the abundances of $(SiO)_2$ and $(SiC)_2$, which remain depleted due to thermal disruption until about 700 days. With fewer nucleation sites, dust formation at early times when the ejecta is warmer would be much more rare than at later times, after the ejecta has cooled appreciably, a result that is inline with the smaller abundance of warm dust discovered by *Herschel* in SN 1987A.

5. Summary and Conclusions

Our model ejecta does condense SiC across a wide range of compositions and initial conditions. Although we have not modeled the condensation of dust, the formation of the stable $(SiC)_2$ molecule is significant as a seed nucleus for the formation of solids or coagulated onto a larger dust grain. Based on our results, we can state the following points:

1. The C/Si ratio in the gas has a direct effect on the abundance of $(SiC)_2$ in the gas. This abundance is maximized when the ratio is near or less than unity, which matches the prediction from Deneault et al. (2003).
2. The $(SiC)_2$ molecule preferentially condenses at low temperatures, so a quickly cooling ejecta is preferential for dust condensation at early times compared to a slowly cooling gas.
3. The highest abundance of SiC occurs when the C/Si ratio is near unity, but the initial density of a cloud governs whether a cloud with a C/Si ratio of less than or greater than unity will produce more $(SiC)_2$.
4. The thermal disruption of small molecules strongly effects their abundances at very early times but has very little effect on the abundances at later times (>800 days).

In this study, we do not claim to have pinpointed the specific regions in Type II supernova ejecta in which SiC will definitely condense. We have, however, explored a range of realistic ejecta compositions, densities, and temperatures and hope to have provided a guide to the physical conditions where these grains could likely form.

References

Andreazza, C. M., Vichietti, R. M., & Marinho, E. P. 2009, MNRAS, 400, 1892
Arnett, D., Fryxell, B., & Mueller, E. 1989, ApJL, 341, L63
Cherchneff, I., & Dwek, E. 2009, ApJ, 703, 642
Cherchneff, I., & Dwek, E. 2010, ApJ, 713, 1
Clayton, D. D., Deneault, E. A.-N., & Meyer, B. S. 2001, ApJ, 562, 480
Clayton, D. D., Liu, W., & Dalgarno, A. 1999, Sci, 283, 1290
Clayton, D. D., & Nittler, L. R. 2004, ARA&A, 42, 39
De Looze, I., Barlow, M. J., Swinyard, B. M., et al. 2017, MNRAS, 465, 3309
Deneault, E. A.-N., Clayton, D. D., & Heger, A. 2003, ApJ, 594, 312
Deneault, E. A.-N., Clayton, D. D., & Meyer, B. S. 2006, ApJ, 638, 234
Ercolano, B., Barlow, M. J., & Sugerman, B. E. K. 2007, MNRAS, 375, 753
Fesen, R. A. 2001, ApJS, 133, 161
Gall, C., Hjorth, J., Watson, D., et al. 2014, Natur, 511, 326
Hammer, N. J., Janka, H.-T., & Müller, E. 2010, ApJ, 714, 1371
Kifonidis, K., Plewa, T., Janka, H.-T., & Müller, E. 2003, A&A, 408, 621
Kozasa, T., Dorschner, J., Henning, T., & Stognienko, R. 1996, A&A, 307, 551
Liu, W., & Dalgarno, A. 1996, ApJ, 471, 480
Matsuura, M., Dwek, E., Meixner, M., et al. 2011, Sci, 333, 1258
McElroy, D., Walsh, C., Markwick, A. J., et al. 2013, A&A, 550, A36
Nittler, L. R., Amari, S., Zinner, E., Woosley, S. E., & Lewis, R. S. 1996, ApJL, 462, L31

Nozawa, T., Kozasa, T., Umeda, H., Maeda, K., & Nomoto, K. 2003, ApJ, 598, 785
Rauscher, T., Heger, A., Hoffman, R. D., & Woosley, S. E. 2002, ApJ, 576, 323
Sugerman, B. E. K., Ercolano, B., Barlow, M. J., et al. 2006, Sci, 313, 196
Todini, P., & Ferrara, A. 2001, MNRAS, 325, 726
Wakelam, V., Herbst, E., Loison, J.-C., et al. 2012, ApJS, 199, 21
Wongwathanarat, A., Müller, E., & Janka, H.-T. 2015, A&A, 577, A48
Woosley, S. E., Heger, A., & Weaver, T. A. 2002, RvMP, 74, 1015
Yu, T., Meyer, B. S., & Clayton, D. D. 2013, ApJ, 769, 38